Molecular dynamics study of tensile and piezoelectric responses of cement paste structure modified with single walled carbon nanotubes

Anna LUSHNIKOVA[1], Yago DE SOUZA GOMES[1], Olivier PLE[1]

[1] *Université Savoie Mont Blanc, CNRS, INES, LOCIE, Chambéry, 73000, France*

This work analyzed the effect of the addition of single-wall carbon nanotubes (SWCNTs) on mechanical and electrical properties of cement composites through Molecular Dynamic simulations. To model the atomic structure of the Calcium Silicate Hydrates (C-S-H) gel, Tobermorite 11Å was chosen. SWCNTs type Armchair (3,3) incorporated into the tobermorite structure in four different quantities (0.00%, 1.22%, 2.55% and 4.00% by weight of Tobermorite 11Å) were tested through simulations of applied uniaxial pressure, as well as simulations of applied electrical field, to study the effect of the concentration of carbon nanotubes in the cement composite. Results exhibited a higher tensile strength and a higher Young's Modulus for the model Tob-CNT(4.00wt%) with values of 14.27 GPa and 165.46 GPa, respectively, while the model Tob-CNT(2.55wt.%) showed a stronger converse piezoelectric response with a calculated d_{33} of $8.62 pC/N$.

Keywords: carbon nanotubes, electrical properties, smart cement, sensor

I. INTRODUCTION

Cementitious composites and concrete, in particular, have been playing a very important role in the last decades, being one of the most used materials for structures until now. Questioning the use of concrete today, researchers have worked to improve the characteristics of cementitious composites, by mixing the cement paste with additives. Therefore, the modern engineering community has shown a lot of interest in the development of civil infrastructure systems with new features for materials such as self-condition monitoring.

New additives are currently being studied and the innovation tends to go towards the nanoscale as cement nanomodification allows new structures to be used as a direct additive into the matrix of the cement composite as well as the creation of new superplasticizers with nanoparticles. Carbon allotropes like graphene and carbon nanotubes (CNTs) are used for this study because they have shown very good mechanical, electrical and thermal properties. The enhanced strength of cementitious materials modified with carbon nanotubes is more widely tested. However, previous studies with carbon nanotubes also identified changes in the piezoelectric values of cement matrix. It is therefore a promising method to develop a

"multifunctional smart concrete" that can be designed to provide mechanical resistance, thermal control, self-monitoring and energy management.

According to bibliographic references, a low concentration of CNTs can increase the mechanical properties of cement-based materials [1-7]. Carbon nanotubes also were employed in cementitious materials to induce a piezoresistive effect [8-12]. Azhari, F., & Banthia, N. 2012 [10] modeled cement-based sensors with carbon nanofibers and carbon nanotubes and reported changes in resistivity, with the best result for the hybrid sensor, containing both carbon nanotubes and carbon nanofibers. Zhao, P et al. 2016 [11] performed experimental works in carbon nanotubes dispersed in cement-sand-based piezoelectric composites with concentrations from 0 to 0.9 vol% (volume percentage) and observed an improvement in the piezoelectric properties, with an optimal value for CNT content of 0.6vol%. Gong, H., et al. 2011 [12] prepared cement based piezoelectric composites from Portland cement with the addition of 70vol% of PZT powders and concentrations of modified CNTs varying from 0 to 1.3vol%. They obtained the highest piezoelectric constant d_{33} of 62pC/N for a 0.3vol% concentration of CNT.

This study deals with numerical simulations. In those simulations the dynamics occur by interaction of discrete elements, in our case atoms which are referred as particles. In the case of this study, the number of particles depend of the number of carbon nanotubes embedded into the structure of tobermorite, so it can be various. In ours examples, the number of particles is between 9683 and 9899. These simulations are allowed by the evolution of software programs for molecular modelling, a computational tool that increases in time to time its accuracy in representing physical, chemical and biological characteristics of systems built by molecules and atoms in interaction.

The piezoelectric effect is the polarization induced by applied strain. When compressing or tensioning, the position of atoms changes within the crystal structure, generating a voltage. The polarization along r-axis can be obtained as follows:

$$P_r = \frac{\sum_i^N q_i r_i}{V} \tag{1}$$

Where q_i is the charge of the *i-th* atom, r_i is the *r*-coordinate of the *i-th* atom, *N* is the number of atoms and *V* is the volume.

The converse piezoelectric effect consists in applying an external electric field to generate deformations. It can be represented by matrices [13] to express, for example, a strain as a result of elastic, thermal, electric and magnetic phenomena, by means of a function of the independent variables (stress σ_{kl}, electric field E_k, magnetic field H_l and temperature ΔT) and their corresponding tensors as follows:

$$\varepsilon_{ij} = S_{ijkl}\sigma_{kl} + d_{kij}^T E_k + q_{lij} H_l + \alpha_{ij}\Delta T \tag{2}$$

Where S_{ijkl} is the elastic compliance, d_{kij} piezo-electric, q_{lij} piezo-magnetic and α_{ij} thermal expansion tensors. In addition to this equation, we can express the previous mentioned effects, that are the interest of this work, with another equation excluding the magnetic effect under the form:

$$D_i = d_{ijk}\sigma_{jk} + \epsilon_{ik}E_k + p_i\Delta T \tag{3}$$

Where D_i is the electric displacement field, ϵ_{ik} is the material electric permittivity and p_i is the pyro-electric tensor.

Thuswise, the main purpose of the present work is to establish at the atomic level, an opportunity of cement paste structure modification with CNTs as a nanodispersed additive and their influence on the modified cement matrix structure. For this objective, it is necessary to determine the atomic structure of C-S-H/CNT composite. Knowing the atomic structure, it is possible to manipulate the system of C-S-H/CNT with the purpose of investigation mechanical and electrical properties sensibility of the obtained cement composite.

II. NUMERICAL SIMULATION

Tobermorite, a calcium silicate hydrate mineral, was chosen in this study, as it is the main constituent and consequently the most representative element of cement paste after hydration. There are some subspecies of tobermorite that are classified by their different interlayer spacing (14Å, 11Å and 9Å) and Tobermorite 11Å is the most used model to describe cement paste in molecular dynamic simulations [16]. Its initial structure is a monoclinic structure with vectors $a = 6.735$ Å, $b = 7.385$ Å, $c = 22.487$ Å and the angles between vectors $\alpha = 90°$, $\beta = 90°$, $\gamma = 123.25°$ obtained by Merlino, 1999 [14].

A python code was developed to create the initial configuration system. The general triclinic unit cell basis can be represented in a matrix format as follows:

$$(a\ b\ c) = \begin{pmatrix} a_x & b_x & c_x \\ 0 & b_y & c_y \\ 0 & 0 & c_z \end{pmatrix} \tag{4}$$

$$a_x = A$$
$$b_x = B\ .\hat{A} = B\cos\gamma$$
$$b_y = \left|\hat{A}\ x\ B\right| = B\sin\gamma = \sqrt{B^2 - b_x^2}$$
$$c_x = C\ .\hat{A} = C\cos\beta$$
$$c_y = C.(A\ x\ B)x\ \hat{A} = \frac{(B\ .\ C - b_x c_x)}{b_y}$$
$$c_z = |C\ .\ (A\ x\ B)| = \sqrt{C^2 - c_x^2 - c_y^2}$$

The fractional positions are included in vector format and three loops will extend the positions in cartesian dimensions according to the system size to form a supercell. In this project, Tobermorite 11Å supercells of size 5x5x3 with a total number between 9683 and 9899 atoms were used.

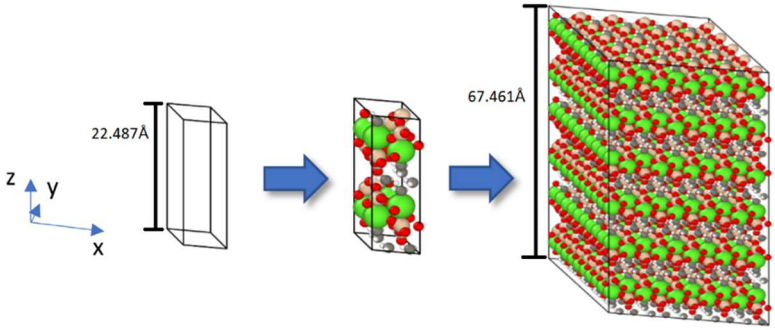

FIGURE 1. Process of creating system configuration

We consider SWCNTs type Armchair (3,3) with length of approximately 70Å. They were aligned to the z direction. First a vacuum in the structure of tobermorite was created. In our study vacuum means the hole created for implement the insertion nanotube in the structure of Tobermorite, in other term, the absence of the atoms in the simulation box keeping the neutral charge of system. It was done by not assigning the unit cells for a giving position in the xy plane, for example, in Figure 2, for the insertion of 1 CNT the unit cells where $x = 3$ and $y = 3$ were ignored in the code. It can be interesting if the geometry of the unit cell, e.g. the cross section is comparable to the hole diameter one wants to use. Other ways of inserting CNT in tobermorite exist, such as the one used by Eftekhari & Mohammadi 2015 [15], in which a zero-diameter cylindrical hole is gradually indented, pushing the atoms backwards, to avoid bond breaks and bonds formation.

Systems with 0.00%, 1.22%, 2.55% and 4.00% of CNT by weight (wt%) of Tobermorite 11Å were prepared (Figure 3). Those concentrations are calculated straightforward by multiplying atomic mass by the number of atoms in the system.

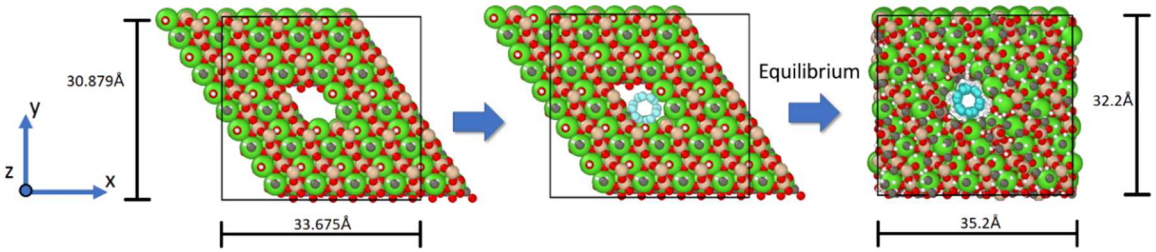

FIGURE 2. Schematic process of inserting a carbon nanotube into Tobermorite 11Å supercell

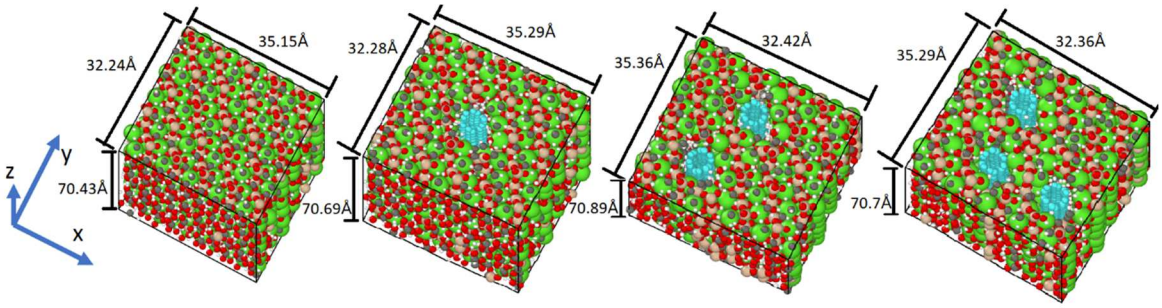

FIGURE 3. Four systems used in the simulations, of the constructed CNT-reinforced Tobermorite 11Å after thermalization

After preparing an Armchair (3,3) CNT we apply Tersoff potential to rule the interaction between carbon atoms. The same procedure is followed with the supercell of Tobermorite 11Å. Interatomic potential energy will result from the sum of all types of atomic interaction, which in our study are described by Buckingham, Stillinger-Weber, core-shell Spring and Coulomb Potential for the atoms within tobermorite structure. Lennard-Jones Potential was used to describe interaction between atoms of tobermorite and CNT [15-17].

III. RESULTS

Periodic boundary conditions were utilized to mimic a bigger system and avoid the boundary effect. A minimization is performed, followed by an NPT ensemble at zero pressure, 300K and a time step of 1 femtosecond to control temperature and pressure of simulation box.

The Young's Modulus of the built model is assessed and compared with the literature (Tables 1 and 2). After equilibration of the system, the length of the simulation box in the z direction is saved as the initial length, before starting deformation through a uniaxial tension applied to the structure by constraining one side of the system and deforming the opposite side with a strain rate of 0.00001/fs.

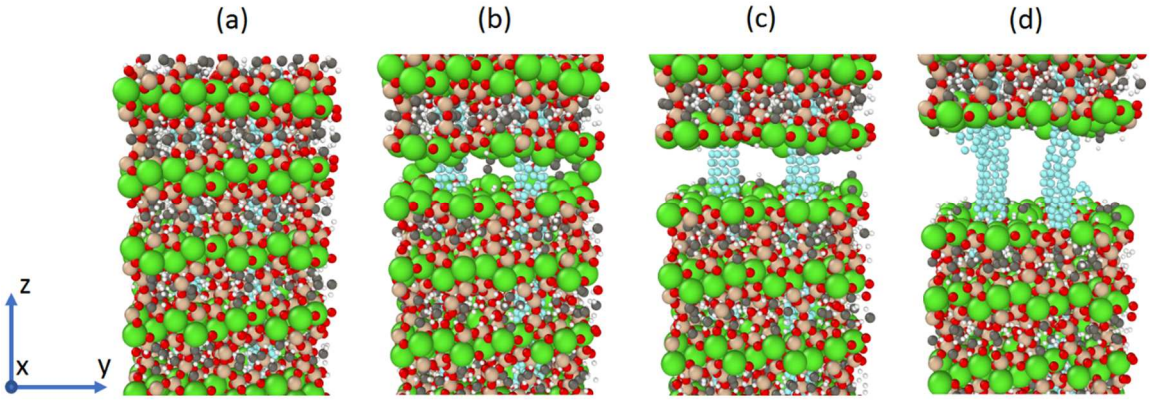

FIGURE 4. Tobermorite 11Å with 2.55wt.% of CNT tensioned along its longitudinal direction at a) strain = 0.0; b) strain = 0.125; c) strain = 0.15; d) strain = 0.25

TABLE 1. Calculated Young's Modulus of Tobermorite 11Å

Tobermorite 11Å	Young's Modulus (GPa)	Method
This work	114.50	Molecular Dynamics
Dharmawardhana et al. [18]	103.25	Molecular Dynamics
Lushnikova [16]	78.39	Molecular Dynamics
R. Shahsavari et al. [19]	82.82	Ab initio

TABLE 2. Calculated Young's Modulus of SWCNT

SWCNT	Young's Modulus (TPa)	Method
This work	1.17	Molecular Dynamics
Wang et al. [20]	1.28-1.48	Molecular Dynamics
Lushnikova [16]	0.510	Molecular Dynamics
X. Lu, Z. Hu [21]	0.989–1.058	Finite Element Analysis
P Subba Rao [22]	1.22-1.28	Finite Element Analysis

After testing Tobermorite 11Å and CNT (3,3) individually, the same tensile test is now imposed to combined Tobermorite 11Å + CNT to evaluate the effect of CNT concentration in the tensile resistance of Tobermorite 11Å. The results for Youngs Modulus, tensile strength and the evolution of stress due to applied strain for the Tobermorite-CNTs models are presented at Table 3 and Figure 5 respectively. The first peak of stress at 0.1 strain (Figure 5) indicates the breaking of bonds in tobermorite atoms (Figure 4b) then the stress increases again but this time tensioning basically only the CNTs (Figure 4c) until the rupture of CNTs at around 0.25 of strain (Figure 4d).

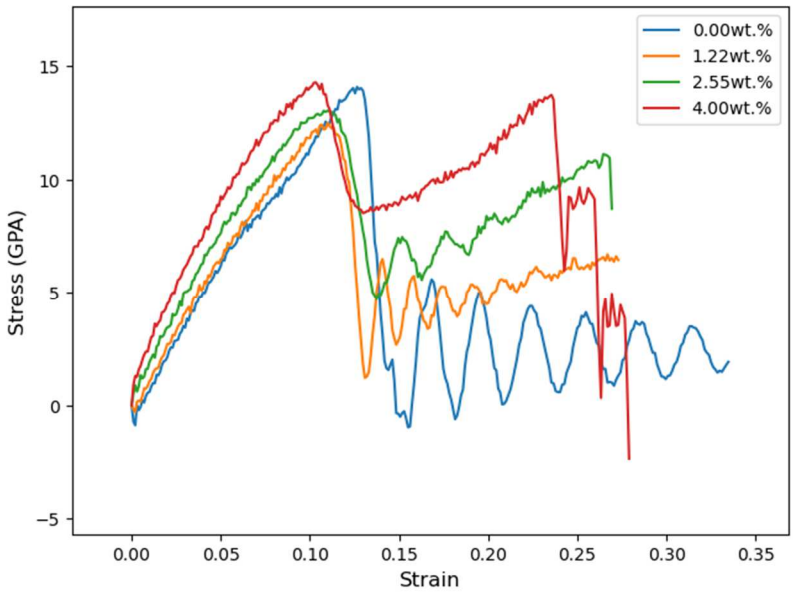

FIGURE 5. Tensile stress vs strain of tobermorite-CNT in z direction

TABLE 3. Young's Modulus and Tensile strength of tobermorite-CNT samples

Model	Young's Modulus (GPa)	Tensile Strength (GPa)
Tobermorite 11Å	114.05	14.07
tob-CNT(1.22wt.%)	139.98	12.49
tob-CNT(2.55wt.%)	148.76	13.03
tob-CNT(4.00wt.%)	165.46	14.27

The converse piezoelectric is simulated. After equilibrating the system, the lengths of the simulation box are followed during the application of an external electric field of 250MV/m oriented in the z-direction. The comparison on the evolution of the box length in z direction for the four systems is presented in Figure 6.

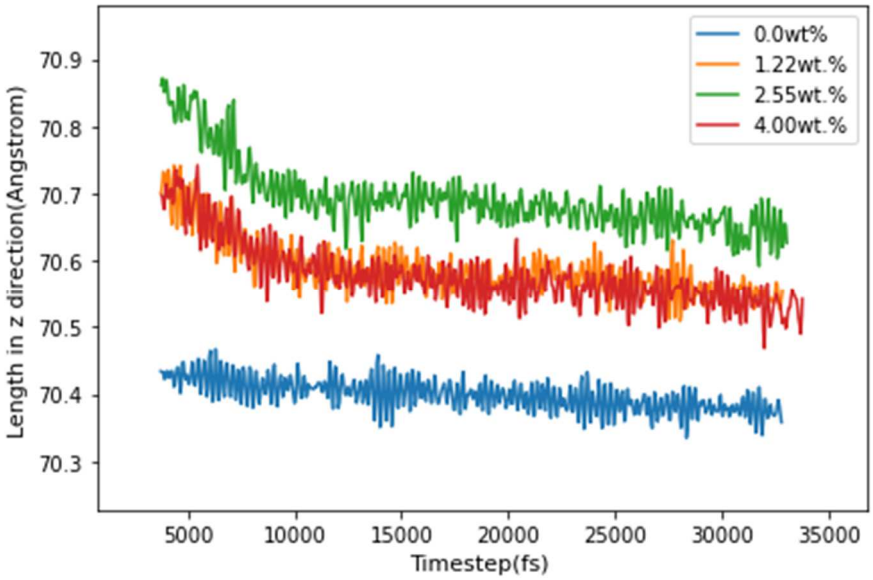

FIGURE 6. Evolution of cell size with different CNT concentrations

The strain tensor ε_{ij} was calculated between steps 4,000 and 10,000 of the simulation. The deformation was a result of the application of an electric field of 250MV/m in the z direction. Considering that there was no external stress applied and no temperature increment, the equation (2) of conversed piezoelectric effect in a triclinic structure can be represented by:

$$\varepsilon_{ij} = d_{ijk}^{T} E_k \tag{5}$$

Which can be solved for d_{33} yielding:

$$\varepsilon_3 = d_{33} * 250MV/m \tag{6}$$

TABLE 4. Piezoelectric constant d_{33} for each of the four samples

Sample	0.00wt.%	1.22wt.%	2.55wt.%	4.00wt.%
$d_{33}(pC/N)$	1.12	6.48	8.62	6.14

IV. DISCUSSION

The ultimate tensile strength is lower for the models Tob-CNT (1.22wt.%) and Tob-CNT (2.55wt.%) than for the Tobermorite 11Å alone, and the model Tob-CNT (4.00wt%) have a higher tensile strength, reaching 14.27 GPa (Table 5). Although the lower values of maximum tensile strength for the models Tob-CNT (1.22wt.%) and Tob-CNT (2.55wt.%), all samples of CNT embedded

tobermorite displayed a higher Young's Modulus. That indicates a probable earlier rupture. The first peak of stress is reached at a lower strain the more CNTs the samples have, what can be explained by the voids of tobermorite made for the insertion of CNT, as the first peak of stress correspond to the collapse of tobermorite (0.1 strain), while the CNTs will collapse afterwards (strain between 0.25 and 0.3), which is illustrated by the multiple peaks in Figure 5. Despite the separated ruptures in the model (first rupture of tobermorite and then rupture of CNT) when translating the nanoscale to the real scale, these two types of rupture should not be that separated. This result can be interpreted as indication of change in the overall strain of rupture and in the overall material's ductility.

In the piezoelectric test, the samples follow a deformation due to the application of an electric field. The box length oriented in the same direction (z) of the electric field is analysed, which correspond to the piezoelectric constant d_{33}. Tob-CNT (2.55wt.%) presented a higher deformation among the models, of 0.002155 strain. The samples containing 1.22 wt.% and 4.00 wt.% experienced a similar deformation while the model with no CNTs had a weak response to the applied electrical field, compared to the other samples.

V. CONCLUSION

In this work, the effect of the addition of carbon nanotubes into cement composites was investigated by means of molecular dynamics simulation, where Tobermorite 11Å was chosen to represent C-S-H gel, being combined with single-wall carbon nanotubes type Armchair (3,3) in four different concentrations and subjected to a tensile test in z direction with a strain rate of 0.00001/ps and, separately, subjected to an electrical field of 250MV/m in z direction.

The tensile stress-strain curves show a higher tensile strength and a higher Young's Modulus for the model Tob-CNT (4.00wt%). The more CNTs are present in the model, the lower is the strain in which the sample reaches first peak, that correspond to the collapse of Tobermorite 11Å. The models with CNTs will have more than one peak, as the stress will increase again after the collapse of tobermorite, until the rupture of the carbon nanotubes, what can indicate a more ductile behavior in the large scale. The converse piezoelectric effect was analyzed following the deformation in the simulation box after the applied electrical field. The results showed a stronger converse piezoelectric response for the sample with 2.55 wt.% with a d_{33} of $8.62 pC/N$.

ACKNOWLEDGEMENT

This work was performed thanks to the financial support of the laboratory LOCIE from Université Savoie Mont Blanc.

REFERENCES

[1] Cerro-Prada, E., Pacheco-Torres, R., Varela, F., 2021. Effect of multi-walled carbon nanotubes on strength and electrical properties of cement mortar. Materials 14, 1–13. doi:10.3390/ma14010079

[2] Li, G.Y., Wang, P.M., Zhao, X., 2005. Mechanical behavior and microstructure of cement composites incorporating surface-treated multi-walled carbon nanotubes. Carbon 43, 1239–1245. doi:10.1016/j.carbon.2004.12.017

[3] Hawreen, A., Bogas, J.A., 2019. Creep, shrinkage and mechanical properties of concrete reinforced with different types of carbon nanotubes. Construction and Building Materials 198, 70–81. doi:10.1016/j.conbuildmat.2018.11.253

[4] Lu, L., Ouyang, D., Xu, W., 2016. Mechanical properties and durability of ultra high strength concrete incorporating multi-walled carbon nanotubes. Materials 9. doi:10.3390/ma9060419

[5] Hu, S., Xu, Y., ... Guo, J., 2020. Modification effects of carbon nanotube dispersion on the mechanical properties, pore structure, and microstructure of cement mortar. Materials 13. doi:10.3390/ma13051101

[6] Lushnikova, A., Zaoui, A., 2017. Improving mechanical properties of C-S-H from inserted carbon nanotubes. Journal of Physics and Chemistry of Solids. doi:10.1016/j.jpcs.2017.02.010

[7] Lushnikova, A., Zaoui, A., 2018. Influence of single-walled carbon nantotubes structure and density on the ductility of cement paste. Construction and Building Materials 172, 86–97. doi:10.1016/j.conbuildmat.2018.03.244

[8] Yu, X., Kwon, E., 2009. A carbon nanotube/cement composite with piezoresistive properties. Smart Materials and Structures 18. doi:10.1088/0964-1726/18/5/055010

[9] Saafi, M., Gullane, A., ... Sadeghi, F., 2018. Inherently multifunctional geopolymeric cementitious composite as electrical energy storage and self-sensing structural material. Composite Structures 201, 766–778. doi:10.1016/j.compstruct.2018.06.101

[10] Azhari, F., Banthia, N., 2012. Cement-based sensors with carbon fibers and carbon nanotubes for piezoresistive sensing. Cement and Concrete Composites 34, 866–873. doi:10.1016/j.cemconcomp.2012.04.007

[11] Zhao, P., Wang, S., ... Wang, X., 2016. Properties of cement–sand-based piezoelectric composites with carbon nanotubes modification. Ceramics International 42, 15030–15034. doi:10.1016/j.ceramint.2016.06.153

[12] Gong, H., Zhang, Y., ... Che, S., 2011. Preparation and properties of cement based piezoelectric composites modified by CNTs. Current Applied Physics 11, 653–656. doi:10.1016/j.cap.2010.10.021

[13] Mainprice, D., 2005. The tensors useful for geophysics and estimation of anisotropic polycrystalline physical properties PART I : The tensors useful for geophysics A) Tensors of physical properties of crystals B) Field tensors C) Cartesian Reference Frames.

[14] Merlino, S., Bonaccorsi, E., Armbruster, T., 1999. Tobermorites: Their real structure and order-disorder (OD) character. American Mineralogist 84, 1613–1621. doi:10.2138/am-1999-1015

[15] Eftekhari, M., Mohammadi, S., 2016. Molecular dynamics simulation of the nonlinear behavior of the CNT-reinforced calcium silicate hydrate (C-S-H) composite. Composites Part A: Applied Science and Manufacturing 82, 78–87. doi:10.1016/j.compositesa.2015.11.039

[16] Lushnikova, A., 2017. Laboratoire Génie Civil et géo-environnement Amélioration des propriétés mécaniques du carbone : une étude par la dynamique moléculaire.

[17] Selvam, R.P., Subramani, V.J., Murray, S., 2009. Potential Application of Nanotechnology on Cement Based Materials. Structure 142.

[18] Dharmawardhana, C.C., Misra, A., ... Ching, W.Y., 2013. Role of interatomic bonding in the mechanical anisotropy and interlayer cohesion of CSH crystals. Cement and Concrete Research 52, 123–130. doi:10.1016/j.cemconres.2013.05.009

[19] Shahsavari, R., Buehler, M.J., ... Ulm, F.J., 2009. First-principles study of elastic constants and interlayer interactions of complex hydrated oxides: Case study of tobermorite and jennite. Journal of the American Ceramic Society 92, 2323–2330. doi:10.1111/j.1551-2916.2009.03199.x

[20] Wang, Y., 2005. Simulation of the elastic response and the buckling modes of single-walled carbon nanotubes. Computational Materials Science 32, 141–146. doi:10.1016/j.commatsci.2004.08.005

[21] Lu, X., Hu, Z., 2012. Mechanical property evaluation of single-walled carbon nanotubes by finite element modeling. Composites Part B: Engineering 43, 1902–1913. doi:10.1016/j.compositesb.2012.02.002

[22] Rao, P.S., Anandatheertha, S., ... Gopalakrishnan, S., 2015. Estimation of mechanical properties of single wall carbon nanotubes using molecular mechanics approach. Sadhana - Academy Proceedings in Engineering Sciences 40, 1301–1311. doi:10.1007/s12046-015-0367-5